Low dimensional silicon to enable silicon photonics

O. Anopchenko, P. Bettotti, M. Cazzanelli, N. Daldosso, L. Ferraioli, Z. Gaburro, R. Guider, D. Navarro-Urrios, A. Pitanti, S. Prezioso, R. Spano and L. Pavesi

Nanoscience Laboratory,
Department of Physics, University of Trento,
via Sommarive 14, 38050 Povo (Trento) Italy.

Abstract

In this chapter we will review the photonic applications of nanostructured silicon. As we change the dimensionality of silicon very fascinating and new optical properties of the material appear. In particular, light emission starts to be a very efficient process in nanostructured silicon and light emitting diodes with efficiency in excess of 1% have been fabricated. Optical amplification has been also observed when silicon nanocrystals are embed into a dielectric matrix. In addition to electronic property variations, nanostructured silicon can be also used as a nanodielectric material. Some examples will be discussed where photonic Bloch oscillations, photonic Zener tunnelling and high quality microcavities are demonstrated.

1 Introduction

Low dimensional silicon is a fascinating material which still has many unfold properties. The main motivation to study silicon comes from its success and dominance in modern technology, especially in microelectronics. Indeed nanometer sized transistors are now switching in computers at working frequency exceedingly few GHz. Convergence between microelectronics and telecommunications is looked for in order to couple the computing power

of microprocessor with the transmission power of optical fibers. In this effort, merging of various semiconductor technologies is attempted in order to improve on one side the optical properties of microelectronic materials and, on the other side, to reduce the cost of photonic devices. With this respect silicon photonics is playing a key role. We have already reviewed in the past several aspects of this emerging technology [1]. In this chapter we aim to give an overview of our recent work towards the exploitation of low dimensional silicon to tune on one side its electronic properties and on the other side its dielectric properties and, thus, allows for new phenomena and device concepts.

Let us define which dimensional scale we are concerned with. If one computes the De Broglie wavelength of electrons in silicon one notices that it is about 5 nm. So in this chapter we are concerned with very tiny amount of silicon of a few nanometer in size, named silicon nanocrystals (Si-nc).

2 Silicon nanostructures

The first motivation to the study of Si-nc was the hope to get luminescent silicon [2]. In fact silicon has an indirect band-gap which causes a very long radiative lifetime (ms) for excited electron-hole pairs. Competing non-radiative recombinations prevail and cause most of the excited electron-hole pairs to recombine non radiatively. In addition, when the number of excited electron-holes increases other non-radiative recombination processes start to play a role. Both are dependent on the density of excess free carriers and dominate the recombinations for heavily excited or doped silicon.

In Si-nc, the radiative recombination rate is increased by quantum confinement. Another effect improves the emission efficiency of Si-nc: the spatial localization of excited electron-hole in a small region of the sample. If this region has a luminescence killer center, the nanocrystal is dark. On the contrary if it is free of killer centers, the nanocrystal is bright and the excited electron-hole recombines radiatively, even though with a long lifetime. In this case the Si-nc has an internal quantum efficiency of 100%, while the system of Si-nc reaches an efficiency of about 10-50 % due to the average between dark and bright Si-nc.

2.1 Luminescence

Si-nc are formed by deposition of a Si-rich silicon oxide followed by a thermal treatment which causes a phase separation between Si-nc and silica. Room temperature emission in Si-nc is routinely observed independently on the

preparation method. The emission is usually characterized by a first band centered at about 500 nm whose position is independent on the processing parameters used to form the Si-nc and a second band in the wavelength range 600-900 nm whose exact spectral position depends strongly on the process parameters (Fig. 1). The first band is defect related and can be quenched by post-growth passivation with hydrogen. It is absent in sample of high quality. The second band is related to the presence of Si-nc: when the Si-nc size decreases due to a low Si-content in the deposited film or to a low annealing temperature treatments the emission band shifts to the blue. On the contrary for high Si-content in the film or high annealing temperature the emission band shows a red-shift.

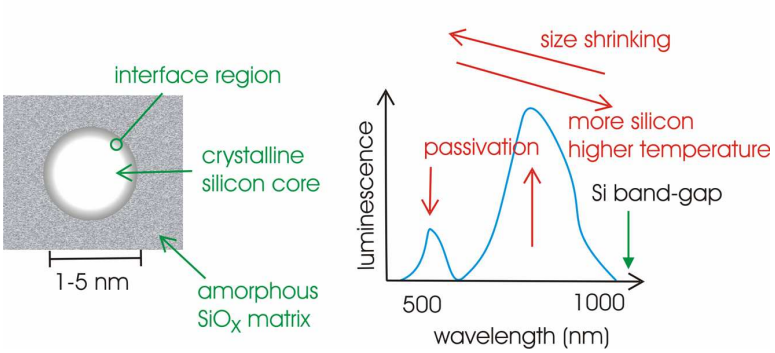

Figure 1: Schematic diagram of a Si-nc (left) and of the corresponding emission spectrum (right). The influence of the various processing parameters on the emission spectrum is shown by the arrows

2.2 Electroluminescence

From a device point of view, photoluminescence is interesting but much more appealing is electroluminescence where light is generated by current injection into the Si-nc [3]. Here the problem is tough since carriers have to pass through a dielectric to excite the Si-nc. Indeed in most of the reported device the electroluminescence is produced either by black-body radiation (the electrical power is converted into heat which raises the sample temperature which, in turn, radiates) or by impact excitation of electron-hole pairs in the Si-nc by energetic electrons which tunnel through the dielectric by a Fowler-Nordheim process (see Fig. 2). Electron-hole pairs excited in this way recombine radiatively with an emission spectrum which is very similar to that obtained by photo-luminescence. The problem with impact

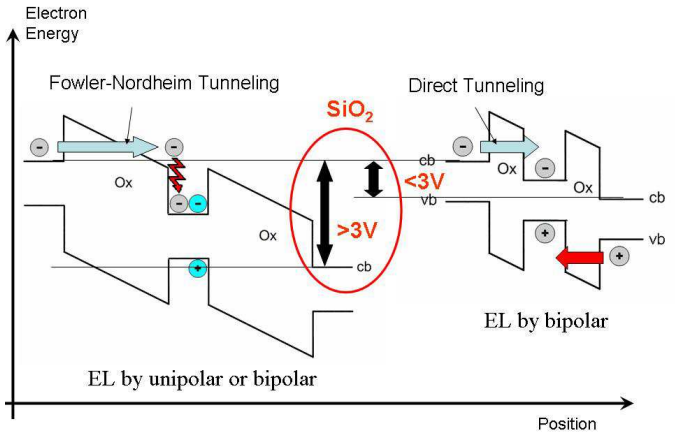

Figure 2: Schematic view of the process of generation of electron-hole pairs in silicon nanocrystals by impact excitation (left) or direct tunnelling (right). Note the different bias which should be used in the two cases. cb or vb refer to the conduction or valence band-edges, while Ox refers to the silicon oxide barrier.

excitation is its inefficiency (maximum quantum efficiency of 0.1%) and the damage it induces in the oxide due to the energetic electron flow. To get high electroluminescence efficiency one should try to get bipolar injection. What most impedes this is the fact that the effective barrier for tunnelling of electrons is much smaller that the one for holes (see Fig. 2. That such separate tunnelling of electrons and holes is possible is well known in the literature (see e. g. [4] or [5]). We are now working on a new injection scheme which aims to control the injection rate of electrons and holes by using band-gap engineering.

2.3 Absorption and refractive index

In order to exploit the optical properties of Si-nc in photonics another parameter of paramount importance is the refractive index. A simple approximation would be to assume an effective average between the ones of silicon and of silica.

However this simple scheme is valid to get a rough estimate but fails when accurate values are needed. In fact, the embedding matrix is not simply composed by SiO_2 and the clustering of excess Si into Si-nc influences the refractive index value. Figure 3 shows that the refractive index

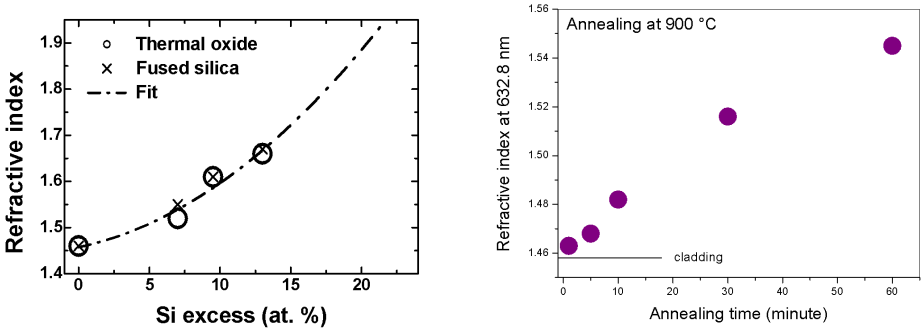

Figure 3: (left) Refractive index as a function of the Si excess. The values obtained by m-lines measurements at 633 nm have been interpolated by a polynomial fit. From Ref. [6]. (right) Samples obtained by sputtering with a Si excess = 6-7% annealing temperature 900 ^{0}C. Refractive index measured at 633 nm for various annealing times. From Ref. [7].

increases as the phase separation between silicon and silica proceeds. In addition, nitrogen is usually found in PECVD deposited Si-nc. This causes the formation of a silicon-oxynitride layer or of a three component matrix with Si, SiO_2 and Si_3N_4. The presence of nitrogen in the film increases the refractive index of the layer significantly.

2.4 Waveguides

The large refractive index of the Si-nc rich layer allows their use as core material in optical waveguides. One of the most important parameter in these waveguides is the propagation losses. Signal light which travels trough the waveguide can loose power due to various mechanisms: direct absorption in the Si-nc, scattering due to roughnesses at the core boundaries (both between the core/cladding interface and at the stripe edges), radiation into the substrate, scattering due to the composite nature of the core layer. Measurements on ridge waveguides formed by ion-implantation and optical lithography have shown that at 780 nm and for sufficiently wide ridges, most of the propagation losses are due to direct absorption in the Si-nc [6]. In fact propagation losses of 11 dB/cm have been measured which can be divided into 2 dB/cm due to Mie scattering, 2 dB/cm due to interface scattering and 9 dB/cm to Si-nc absorption, α. Knowing that $\alpha = N\sigma$ an estimate of the absorption cross section of Si-nc can be obtained: σ_{abs}=5x10^{-19}cm^2. At 1550 nm propagation losses of 2 dB/cm have been reported [7].

2.5 Optical gain

Active devices, such as lasers or amplifiers, need optical gain in the active material. We have found that Si-nc have net optical gain. To measure optical gain, we used the variable stripe length (VSL) method, where the luminescence of Si-nc is used as a probe beam and one looks for enhancement as it propagates in an optically pumped waveguide. Figure 4 shows on

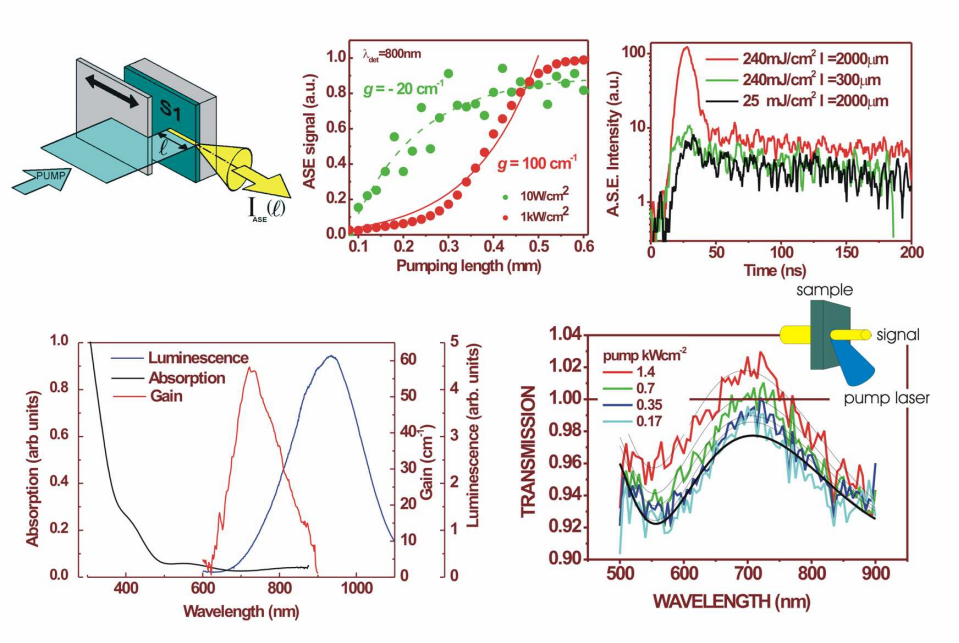

Figure 4: Top-left: schematics of the VSL method. Top-center, amplified spontaneous emission ASE versus the pumping length for two pumping powers at a wavelength of 800 nm and for a PECVD slab waveguide. Data are from Ref. [8]. Top-right: time resolved ASE for various pump power and excited volume. Bottom-left: Summary of the optical properties of Si-nc. Black curve is the absorption spectrum, dashed curve is the gain spectrum, dotted curve is the luminescence spectrum. Data from ref. [8]. Bottom-right: Transmitted intensity as a function of the pump power density. Dark line refers to the transmission of the sample without any pumping. The inset shows the schematic of the experiment. From [9].

the top-left the idea of the VSL method. Losses or gain can be measured depending on the pump power, see Fig. 4 top-center, and by modelling the system within a one dimensional amplifier scheme the gain spectrum can be measured (Fig. 4 bottom-left). [8].

Gain is also observed in signal amplification experiments (Fig. 4 bottom-

right) [9]. We used a thin layer of Si-nc formed on a transparent quartz substrate. As the pumping rate is increased the transmission intensity increases too. For 1.4 kWcm^{-2}, the transmitted intensity is larger than 1. This means that overall amplification of the signal beam is achieved: the transmitted intensity is larger than the incident intensity even accounting for the losses through the substrate.

A summary of the optical properties of the Si-nc system is shown in Fig. 4 bottom-left, where absorption, gain and luminescence spectra are compared. It is worth noticing the large energy difference between absorption and emission spectra: where absorption is negligible, emission (either stimulated or spontaneous) is strong. Furthermore, the gain spectrum peaks at the high energy side of the luminescence spectrum. These data can be explained with a four-level model of gain where lattice relaxation of Si=O double bonds at the interface of the Si-nc provides the energetic for the four level model. Shifts between luminescence and gain point to a different nature of the active centers in the two cases: either two populations of Si-nc are present in the system or interface radiative recombination is responsible of gain and band-to-band recombination in large S-nc is responsible for luminescence. The exact model is still under discussion in the literature.

2.6 Non-linear optical properties

Nonlinear photonic materials are widely used in many key-devices for the telecom industry such as switches, routers, wavelength converters. As an example, optical logic gates realized with nonlinear Mach-Zehnder interferometer (MZI) offer a very attractive feature for mass-manufacturing such as scalability and flexibility. Si-nc are very promising material for nonlinear applications. By using z-scan techniques we performed a detailed analysis of the non-linearities of Si-nc at 1550 nm.

Representative experimental data are shown in Figure 5. It was found a positive z-scan trace (positive nonlinear refraction index, n_2). This kind of nonlinearity is due to the bound electronic response. n_2 is estimated of the order of 10^{-13} cm^2/W. In addition a nonlinear absorption is also observed, whose nonlinear absorption coefficient β is in the range of - $(10^{-9} - 10^{-8})$ cm/W. We found that n_2 is higher for higher n_0. n_0 is related to the Si-nc sizes and density, thus the nonlinearities increase as the Si-nc size and density increase. This effect is in contrast with expectations dictated by quantum confinement effects, where it is predicted that the nonlinearities increase as the nanocrystal size decreases. A probable explanation is that at 1500 nm the nonlinearities are also affected by the dielectric mismatch

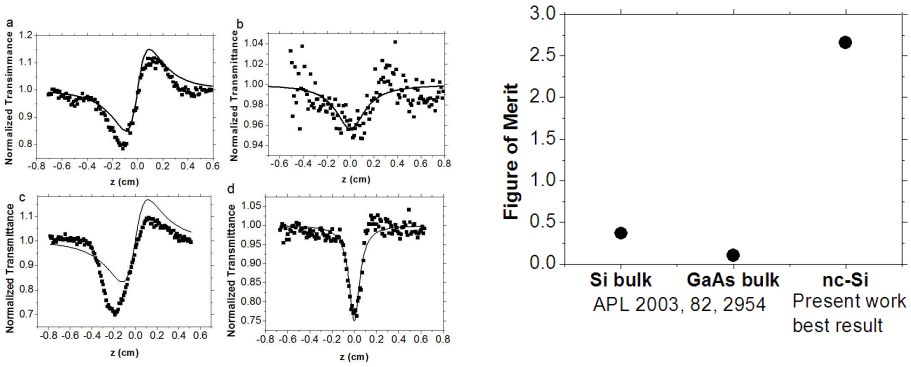

Figure 5: (left) Representative z-scan traces for a sample with 1 nm large Si-nc: closed (a) and open (b) aperture; and for a sample with 4 nm large Si-nc: closed (c) and open (d) aperture. Both the samples are annealed at 1100 C. The theoretical fitting is also included as a solid curve. The laser had a λ = 1550 nm, 1 kHz repetition rate with 100 fs pulse duration and a peak intensity 6x10^{11} W/cm^2(right) Comparison between F from Si-nc, bulk Si and bulk GaAs at 1550 nm [10].

between the Si-nc and the oxide. The local electric field experienced by the nanocrystals is enhanced compared to the incident field because of the dielectric mismatch. The relative importance of the two effects (dielectric mismatch and quantum confinement) is weighted by the energy at which the nonlinearities are measured. For infrared light, the nonlinearities seem to be largely influenced by the dielectric mismatch.

The material properties with respect to device performances can be assessed by the introduction of the nonlinear figure of merit F = n_2 / $\beta\lambda$ [10]. The estimation of F for our samples have evidenced that the Si-nc show higher F-values than bulk Si and bulk GaAs (Fig. 5). High F values are achieved with low size Si-nc because of their low nonlinear absorption coefficient.

3 Complex dielectric structures

When the dielectric function of a material is purposely varied in a periodic manner, the photon propagation properties in the material are drastically modified. Energy regions, where photon propagation along given directions is permitted or prohibited, appear and the system is described as a photonic crystal. However not only periodic dielectric systems are of interest but also more complex structure where the dielectric function is varied ape-

riodically or randomly. A simple system to produce these complex dielectric structures is porous silicon where one can vary the dielectric function in one dimension by controlling local variation of the porosity [11]. High-Q factor microcavities or multiple coupled microcavities have been grown free standing to allow for transmission experiments. It is very interesting to compare

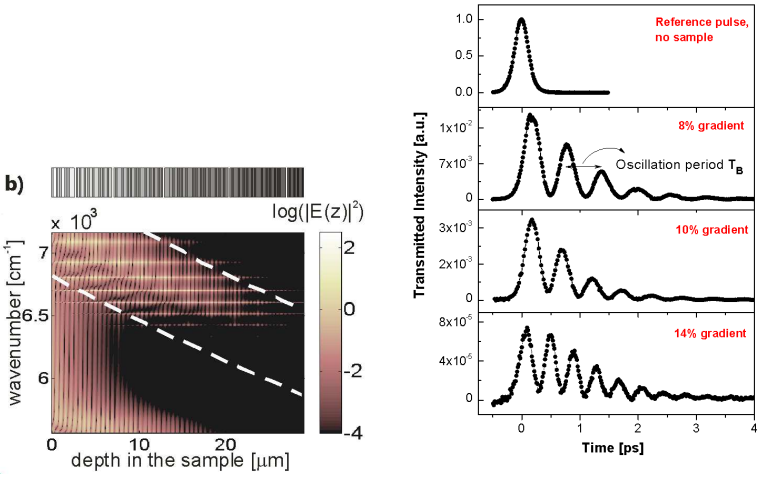

Figure 6: (left) Scattering state maps of an optical superlattice with a 14% optical path gradient applied along the sample. The lines show the tilting in the photonic structures. (right) Time resolved transmitted intensity of a short photon pulse through a biased optical superlattice. The different panels refer to different samples with an increasing value of the optical path gradient. Note the drop in the transmitted intensity as the gradient increases, which is an evidence of the increased localization of the photons inside the tilted superlattice. The photons get Bragg reflected inside a thinner region as the gradient increases. This is also observed in a decrease of the Bloch oscillation periods. From Ref. [12]

single microcavity and multiple coupled microcavities, with their electronic counterpart: single isolated quantum well and superlattices. In both case the presence of a layer within barrier materials (DRB in the photonic case, high band-gap material in the electronic case) cause the appearance of a state in an otherwise forbidden energy region. In both case, if one stacks more cavities/wells coupling of the single states occurs and a miniband is formed where photons/electrons can freely move. For this reason, we call the coupled microcavity system *optical superlattice*. If one uses this analogy further, it is tempting to try to reproduce electrical phenomena with optics. The still missing ingredient is the optical analogue of an electric field: i. e. an external means to tilt the energy band of the optical superlattice.

Since in a microcavity the resonance wavelength is λ=nd=δ, where d is the physical thickness of the cavity layer, then $\lambda + \Delta\lambda = \delta + \Delta\delta$. Thus if the optical path δ is changed linearly throughout the optical superlattice, this ends-up in a tilting of the optical superlattice miniband [12]. We call $\Delta\delta$ the optical path gradient. This simple reasoning is confirmed by the calculation of the optical superlattice with a gradient. This is shown in Fig. 6, where an optical gradient of 14% induces a significant tilting of the photonic structures. In the first paper about electronic superlattice, it was suggested that

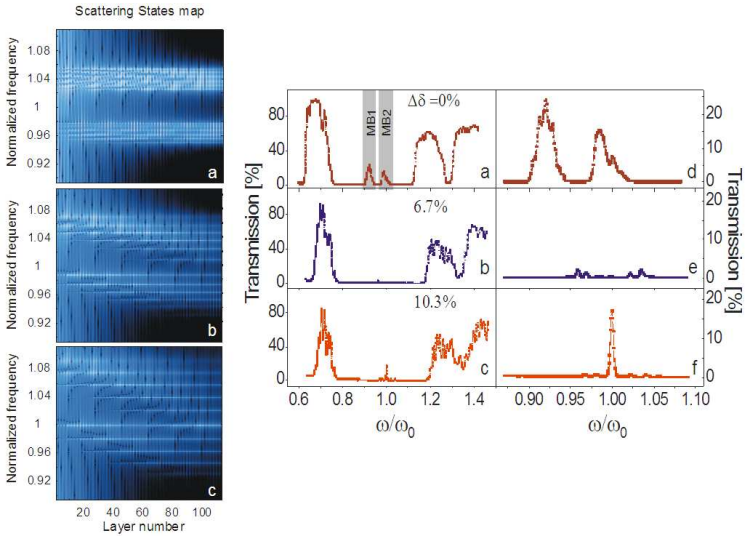

Figure 7: (left) Scattering states map of a two miniband optical superlattices for various optical path gradients. (center and right) Transmission spectra of the optical superlattices: (a) flat band situation $\Delta\delta$ = 0%, (b) $\Delta\delta$ = 6.7%, (c) $\Delta\delta$ = 10.3%, (d) $\Delta\delta$= 18 %. (e)–(h) A zoom of the wide range spectra around the miniband region. Resonant Zener tunnelling is observed in (c) and (g) as an enhanced transmission peak in the center of the minigap. From [14].

the demonstration of the formation of a miniband of electronic state was the observation of electronic Bloch oscillations [13]. These are due to the reflections at the band-edges of electrons accelerated in a static electric field. The possibility of tilting the photonic miniband in an optical superlattice makes possible the observation of photonic Bloch oscillations. Photons are Bragg reflected by the tilted miniband edges which is observed as the appearance of a train of pulses when a short pulse is injected into the photonic structures. Figure 6 reports the first measurements of this oscillating light produced by a single incoming pulse [12].

The analogy between electrons and photons can be tested even further if

one considers now the effect of a bias (optical path drift) on a two miniband optical superlattices (Fig. 7 left) [14]. For zero bias, the photonic structure is characterized by two minibands of propagating states. A transmission experiment will measure two transmission bands in the photonic band-gap. If one starts to bias the optical superlattice (increase the optical path gradient) a ladder of localized photonic states appears. A transmission experiment will measure a drastic drop in the transmission with the appearance of a series of equally spaced weak peaks. If the bias is increased even further the first Wannier Stark ladder state of one miniband resonantly couples with the last Wannier Stark state of the other miniband. This coupling causes the formation of an extended state trough the whole structure and photons can tunnel through the sample. Indeed transmission experiments show that a strong peak appears. This fact is a manifestation of the resonant photonic Zener tunnelling, which is experimentally shown in Fig. 7 right and reported in Ref. [14].

4 Conclusion

In this chapter we have shown some of the many applications of Si-nc in photonics. Both quantum size effects, the new chemistry which occurs at the Si-nc surface, the tunability of the dielectric functions by changing the composition of the systems, all allows to generate new phenomena which can be eventually used to add new functionalities to silicon and enables silicon photonics.

Acknowledgement

We acknowledge the help of many co-workers both from national and from international collaboration. They can be recognized in the cited literature. The research here discussed has been made possible by the financial support of many projects: FP6-IST SINERGIA, FP6-NMP SEMINANO, FP6-IST PHOLOGIC, FP6-TMR POLYCERNET, FP6-IST LANCER, FIRB RBNE01P4JF, FIRB BNE012N3X and COFIN (2004023725).

References

[1] *Silicon Photonics,* edited by Lorenzo Pavesi and David Lockwood, Topics in Applied Physics vol. 94 (Springer-Verlag, Berlin 2004).

[2] Ossicini Stefano, Pavesi Lorenzo, Priolo Francesco *Light Emitting Silicon for Microphotonics*, Springer Tracts in Modern Physics, Vol. 194 (Springer-Verlag, Berlin 2003).

[3] Z. Gaburro and L. Pavesi, *Light emitting diodes for Si integrated circuits*, in Handbook of Luminescence, Display Materials and Devices, vol 3. Display devices, edited by H. S. Nalwa and Lauren Shea Rohwer (American Scientific Publishers, Stevenson Ranch, USA 2003) pag. 101-127.

[4] J. Cai and C.-T. Sah, J. Appl. Phys. **89**, 2272 (2001).

[5] R. J. Walters, G. I. Bourianoff, H. A. Atwater Nature Materials **4**, 143 (2005).

[6] P. Pellegrino, B. Garrido, C. Garcia, J. Arbiol, J.R. Morante, M. Melchiorri, N. Daldosso, L. Pavesi, E. Schedi and G. Sarrabayrouse, J. Appl. Phys. **97**, 074312 (2005).

[7] N. Daldosso, D. Navarro-Urrios, M. Melchiorri, C. Garca, P. Pellegrino, B. Garrido, C. Sada, G. Battaglin, F. Gourbilleau, R. Rizk, L. Pavesi, IEEE- Journal of Selected Topics in Quantum Electronics **12**, 1607 (2006).

[8] L. Dal Negro, M. Cazzanelli, N.Daldosso, Z.Gaburro, L. Pavesi, F. Priolo, D. Pacifici, G. Franzó and F. Iacona, Physica E **16**, 297 (2003)

[9] L. Dal Negro, M. Cazzanelli, B. Danese, L. Pavesi, F. Iacona, G. Franzó and F. Priolo, J. Appl. Phys. **96**, 5747 (2004).

[10] 9. M. Dinu, F. Quochi and H. Garcia, Appl. Phys. Lett. **82**, 2954 (2003).

[11] O. Bisi, S. Ossicini and L. Pavesi, Surface Science Reports **264**, 1 (2000).

[12] R. Sapienza, P. Costantino, D. Wiersma, M. Ghulinyan, C. J. Oton and L. Pavesi, Phys. Rev. Lett. **91**, 263902 (2003).

[13] L. Esaki, and R. Tsu, IBM J. Res. Dev. **61**, 16 (1970).

[14] M. Ghulinyan, C. J. Oton, Z. Gaburro, L. Pavesi, C. Toninnelli and Diederik Wiersma, Phys. Rev. Lett. **94**, 127401 (2005).